JMRA

Journal of Mechanical Research and Application

Reducing the Airflow Separation Region and Turbulence around the Airfoil using a Body Force

Mohammad Bigdeli [*1], **Gholamreza Tathiri** [2], **Alireza Ansari** [3], **Vahid Monfared** [4]

1. Department of Mechanical Engineering, Zanjan Branch, Islamic Azad University, Zanjan, Iran.

2. Department of Mechanical Engineering, Zanjan Branch, Islamic Azad University, Zanjan, Iran.

3. Department of Mechanical Engineering, Zanjan Branch, Islamic Azad University, Zanjan, Iran.

4[*]. Department of Mechanical Engineering, Zanjan Branch, Islamic Azad University, Zanjan, Iran.

(E-mails: mohammadbigdeli71@gmail.com)

Abstract: This study investigates the flow separation region on NACA 0012 airfoil at a constant Reynolds number using plasma actuators to create a net body force, and therefore controlling the airflow around rigid objects. These actuators are among the most popular methods in active flow control due to their easy installation, very short response time, and very low power consumption. The K-ω SST turbulence model has been used for simulation and numerical analysis of airflow on the airfoil. The lift coefficients are analyzed and investigated from different angles as well as the critical (stall) angle of attack. Obtained results show that with increasing angle of attack, eddy and return flows in the separation region increase and also the lift coefficient at the stall angle decreases sharply, therefore is causing energy loss. The aim of this study is to minimize the flow separation region and eddies so that the separated airflow from the airfoil is again smoothed over the airfoil surface using plasma actuator. Plasma actuator is defined as a UDF code in ANSYS Fluent software as a body force on the airfoil. In which the lift coefficient is increased with the activation of the plasma.

1. Introduction

In this study, a symmetrical airfoil with NACA 0012 characteristic is exposed to air flow at a constant speed at an angle of attack of 0° and the lift coefficient is calculated. In which the angle of attack is increased stepwise. Afterwards, the lift coefficient is recalculated and it is observed that as the angle of attack is increased, the air flow separation zone increases and causes eddies and return flows, and this separation region is undesirable and causes energy losses and damage to the aircraft. At an angle of attack, the flow must be separated from the airfoil and the stall phenomenon must occur. The stalling angle and angles above it are supercritical. At this point, the body force is applied and the fluid flow is reset to the airfoil cross section. The lift coefficient is calculated again, and flight must be possible at the stall angle. Our goal in this study is to minimize return

flows and eddies on the airfoil using plasma actuators. This makes the smaller vortex area and the flow separation occurs with delay. Among the published and available research works related to this discussion, the following important research works are accessible.

Ismailzadeh and Aghazeinali [1] studied the flow around a cylinder under the influence of a rod-plate electro hydrodynamic actuator attached to the surface of the cylinder using the finite element method. They found that by applying an electric field, the fluid flow accelerated in the vicinity of the front half of the cylinder, and as a result of increasing the pressure difference between the front and rear surfaces of the cylinder, the drag coefficient increased. They also showed that the volume of the tail section behind the cylinder and the drag coefficient decreased for the same voltage difference as the input velocity increased [1]. On the other hand, the effects of an electro hydrodynamic actuator on the flow around circular cylinder were analyzed using the FEM. For this aim, after choosing appropriate area and proper boundary conditions, electric field was analyzed numerically and the results were presented and introduced to the governing equations of fluid field as electrical body forces. Then, the influence of ionic wind resulted from the electro hydrodynamic actuator on the fluid velocity, fluid pressure, extended wake behind circular cylinder and also drag coefficient of the cylinder was recalculated and resolved. As well, the fluid flow nearing the wall of frontal surface was accelerated. For the actual arrangement of the electrodes, the pressure difference between the frontal and back of the cylinder was increased and caused the enhancement of drag force logically. However, this presented phenomenon is caused the reduction of the wake region on the cylinder [1].

Leger et al. also examined the effect of DC corona discharge on airflow along a sloping flat plate. The detection of the flow field as well as determination of the velocity distribution using PIV technology showed that without the application of the electric field, the flow is separated at the front edge of the plate and significant wakes are formed at the top of the plate. However, by applying an electric field and corona discharge, the flow lines are diverted to the plate, which, according to the Reynolds number of flow and the slope of the plate, leads to collisions or non-collision of flows with the plate and the number of eddies decreases at the same time. They also found that the effect of corona discharge on flow characteristics was lower in low Reynolds numbers in the form of reduced flow wakes and reduced drag force, and with increasing flow velocity, the effect of corona discharge was reduced [2].

Artana et al. studied the flow control around the cylinder by electro hydrodynamic actuators in the range of 23000 <Re <58000. The following figure shows examples of flow detections in the low speed range (Re~2500), in discharge and non-discharge states. In their experiments, this group observed that after applying an electric field and after a short period of time, the transient zone in the separated boundary layer became closer to the cylinder. Also, the area of eddy formation was greatly disturbed and the vortex areas became so short that it was very difficult to identify them [3]. That is, the modifications of the near wake of a circular cylinder has been analyzed when the flow was perturbed steadily utilizing an electro hydrodynamic (EHD) actuator. Also, two electrodes flush-mounted on the surface of the cylinder were excited with DC power supplies to make a plasma sheet contouring the body. The discharge produced an electric force and changed the physical properties in the fluid layers at close vicinity to the surface. According to the obtained results [3], the plasma sheet reduced the base pressure, modified the size of the mean recirculation region and produced an increase in the shear stresses of the layers bounding the contour of this region [3].

Salmasi et al. studied the numerical and experimental effects of a plasma actuator on the performance of the NEL 0414 airfoil. They showed that the presence of a plasma actuator on the surface of the airfoil and near the start of the separation delays the separation point and increases the airfoil efficiency [4]. That is, plasma actuator is one of the newest devices in flow control techniques which can delay separation by inducing external momentum to the boundary layer of the flow. So a NLF0414 airfoil has been simulated by

experimental and numerical methods in presence of the body force vector induced by a specific plasma actuator [4]. Therefore, the model is carried out numerically and experimentally for a NLF0414 airfoil with the compressible 25 m/s velocity airflow in two different cases: without plasma actuator located on the airfoil and with body force produced by a plasma actuator located on the top of the airfoil to analyze the effect of plasma on the flow passing over it. The results showed that presence of a plasma actuator on the top surface of the airfoil, close to the separation point, transferred the separation point from x=16 mm to x=41 mm at the angle of attack of 18 degrees. This separation delay caused a 35% raise in the ratio of lift to drag coefficient or the efficiency of the airfoil in the same angle of attack [4].

Moreover, some constitutive and required equations have been used for analyzing the present problem [5-10, 14-18]. To validation and comparison of the obtained results, the references of [11, 19] have been utilized.

Jayaraman et al. analyzed a combination model of plasma dynamics and hydrodynamics using the concept of induced thermos fluid by electrical discharge. They modeled the helium DBD in asymmetric geometry using the two-dimensional finite volume method. They found that increasing the size of the lower electrode, increasing the voltage, and decreasing the frequency could increase the average maximum force values, while increasing the dielectric constant of the insulating material reduced the resulting average force [12]. Also, the two-dimensional helium dielectric barrier discharge in an asymmetric geometry has been modeled via a finite volume operator-split sequential approach to efficiently solve the multiscale problem. The two-species plasma simulations revealed that the generation of the unidirectional momentum coupling is primarily affected by the combination of factors such as the asymmetry of the geometric arrangement, the wave form of the applied voltage, the species mobility, and dielectric material. It seems that there are two conditions to obtain higher axial force which is delivered to the neutral fluid increasing the peak value of the cyclic force generation and introducing more asymmetry to the first and second half of the cycle to make the positive part more prominent. Although various parameters are coupled and correlated to each other, the increase in the lower electrode size, applied voltage, and dielectric constant tend to contribute to the first factor, and the decrease in frequency of applied voltage tend to contribute to the second factor. To generate higher force, these parameters including others need to be adequately tuned to accomplish those conditions.

Asada et al. investigated the effect of the DBD plasma actuator generated by an impulsive wave on the airflow around the NACA0015 symmetrical airfoil at Reynolds numbers 44,000 and 63,000 through experiment in a low-velocity wind tunnel. That is, the parameters of DBD (Dielectric Barrier Discharge) plasma actuator with burst wave (duty cycle) have been analyzed using the low speed wind tunnel experiment for airfoil [13]. In which, influence of burst frequency, input voltage sine wave frequency and burst ratio (BR) on the stall control were are studied. The experimental processes were done with the conditions Re = 44,000, and 63,000. The actuator was used to NACA0015 airfoil and then flow fields around the airfoil were visualized by the smoke wire method and pressure around its surface was measured by the multipoint steady pressure measurement [13]. The results shown that within the present experimental conditions, the higher burst frequency and voltage sine wave frequency are more effective in the separation control and the smaller BR (burst ratio) has the stronger separation control capability in spite of less input energy. In the present conditions, the optimum dimensionless burst wave frequency is 9.1 [13]. As a result, the smaller BR has stronger separation control capability in spite of less input energy.
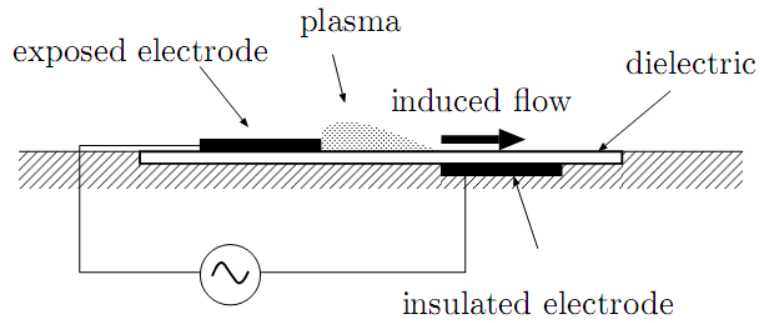
Fig1. Configuration of the DBD plasma actuator [13].

DBD plasma actuator is a small flow control device that can be applied to airfoil stall control, reduction of wall surface friction, etc. It is composed of two electrodes and dielectric as shown in Fig. 1. Plasma is generated by dielectric barrier discharge in the area between the exposed electrode and the dielectric when alternative current high voltage is applied to both electrodes. Plasma is accelerated by electric field and provide atmosphere with momentum. So the flow which velocity is as small as about several m/sec is induced from the exposed electrode to the insulated electrode [13].

Also, the flow separation on NACA 0012 Airfoil has been analyzed at Reynolds number of 3×10^6 in the turbulent state. To do this, the airfoil was first exposed to the airflow at an angle of attack of $0°$ and the lift coefficient was calculated, then the angle of attack was increased by regular steps, followed by a precise increase in angle of attack by one-degree step at an angle of attack of $12°$, and the lift coefficient has been calculated simultaneously. As the results, in an area of airfoil, due to the increasing in angle of attack, the flow is separated from the airfoil, where the lift coefficient decreases sharply and stall occurs. Stall and angles higher than the stall angle is critical and supercritical, making it difficult for the pilot. The aerodynamics of two-dimensional fins was discussed, and also $k - \omega$ SST, Realizable k-ε and Spalart-Allmaras turbulence models were used to study and compare the stall angle in Reynolds number 3×106 using these three turbulence models. Airfoil design and airflow simulation were performed on airfoil using ANSYS Fluent19 analytical software [20].

In this study, it is tried to minimize eddies and return flows with the help of a body force at Reynolds number of 3×10^6 using the K-ω SST turbulent model with the help of ANSYS FLUENT software and numerical analysis. As a result, the lift coefficient should be increased and the stall angle should be delayed.

2. PREVAILING EQUATIONS AND BOUNDARY CONDITION

In this study, an attempt is made to model the flow around the NACA 0012 airfoil modeling and examine geometry meshing and impacts related to plasma actuators. For this purpose, an airfoil is considered in the flow regime and the related equations are solved numerically.

2.1. Continuity and Momentum Equations

To calculate a CFD simulation, the conservation of mass equation and momentum equation are used. The conservation of mass equation is applied to any fluid type such as three-dimensional, viscous or non-viscous, compressible or incompressible flows. The continuity equation shows that if we put a control volume in a fluid area, the mass input and output are equal while no mass generation takes place. So, Equation (1) is as the following [۵],

$$\frac{\partial \rho}{\partial t} + \nabla.(\rho\vec{u}) = S_m \tag{1}$$

Equation (1) is the conservation of mass equation, or continuity equation, where S_m is the source term. Following is the conservation of momentum equation [۵],

$$\frac{\partial(\rho\vec{u})}{\partial t} + \nabla.(\rho\vec{u}\vec{u}) = -\nabla p + \nabla.(\tau) + \rho\vec{g} + \vec{F} \tag{2}$$

In Equation (2) $\rho\vec{g}$ is gravitational body force, p is the static pressure, $\vec{F}$ is the external body force, τ is the stress tensor and its equation is as follows,

$$\tau = \mu\left[(\nabla\vec{u} + \nabla\vec{u}^T) - \frac{2}{3}\right]\nabla.\vec{u}I \tag{3}$$

Where I is the identity matrix and μ is the molecular viscosity. The equation for two-dimensional steady and incompressible flow is as follows [۵],

$$\frac{\partial u}{\partial x} + \frac{\partial v}{\partial y} = 0 \qquad (\text{Continuity equation}) \tag{4}$$

$\rho\frac{Du}{Dt} = -\frac{\partial p}{\partial x} + \frac{\partial\tau_{xx}}{\partial x} + \frac{\partial\tau_{yx}}{\partial y}$ (Momentum conservation in x direction)   (5) $\rho\frac{Dv}{Dt} = -\frac{\partial p}{\partial y} +$

$\frac{\partial\tau_{xy}}{\partial x} + \frac{\partial\tau_{yy}}{\partial y}$ (Momentum conservation in y direction)   (6)

2.2. K-ω SST Turbulence Model

The k-ω SST turbulence model is proposed by Menter [6] in order to combine the precise and robust formulation of the k-ω model (Wilcox) in the near-wall regions with the free-flow independent k-ε model in the far-wall regions. The k-ω SST turbulence model is similar to the standard k-ω model. They are also very accurate for a wide range of boundary layer flow with pressure gradient. This model is widely used in aerospace and turbo machinery. The k-ω SST turbulence model includes a modified vortex viscosity equation to accurately calculate the effects of the transfer of main vortex shear stress [6-8]. The equations for this turbulence model are as follows [6],

$$\frac{D\rho k}{Dt} = \tau_{ij}\frac{\partial u_i}{\partial x_j} + \beta^*\rho\omega k + \frac{\partial}{\partial x_j}\left[(\mu + \sigma_k\mu_t)\frac{\partial k}{\partial x_j}\right] \tag{7}$$

$$\frac{D\rho\omega}{Dt} = \frac{\gamma}{v_t}\tau_{ij}\frac{\partial u_i}{\partial x_j} - \beta\rho\omega^2 + \frac{\partial}{\partial x_j}\left[(\mu + \sigma_\omega\mu_t)\frac{\partial\omega}{\partial x_j}\right]$$
$$+ 2\rho(1 - F_1)\sigma_\omega\frac{1}{\omega}\frac{\partial k}{\partial x_j}\frac{\partial\omega}{\partial x_j} \tag{8}$$

Also, the turbulence stress tensor τ_{ij} considering $\beta^* = \frac{\varepsilon}{k\omega}$ is as follows,

$$\tau_{ij} = -\rho\overline{u_i'u_j'} = \mu_t\left(\frac{\partial u_i}{\partial x_j} + \frac{\partial u_j}{\partial x_i} - \frac{2}{3}\frac{\partial u_k}{\partial x_k}\delta_{ij}\right) - \frac{2}{3}\rho k\delta_{ij} \tag{9}$$

The turbulence vortex viscosity is calculated by Equation (10),

$$v_t = \frac{a_1 k}{max(a_1\omega, \Omega F_2)} \tag{10}$$

In which, a_1=0.31 and Ω is the absolute value of the vorticity. Finally, the F_2 is as the following form,

$$F_2 = tanh\left\{\left[max\left(\frac{2\sqrt{k}}{0.09\omega y}, \frac{500v}{y^2\omega}\right)\right]^2\right\} \tag{11}$$

In Equation (11) y is the distance to the nearest wall. Moreover, β, σ_k, k, σ_ω, ω and γ coefficients are defined as coefficients of the k-ω and k-ε turbulence models, and their relationships are as follows,

$$\beta = F_1\beta_1 + (1-F_1)\beta_2 \ , \gamma = F_1\gamma_1 + (1-F_1)\gamma_2$$
$$\sigma_k = F_1\sigma_{k1} + (1-F_1)\sigma_{k2} \ , \sigma_\omega = F_1\sigma_{\omega 1} + (1-F_1)\sigma_{\omega 2} \tag{12}$$

Where F_1 is obtained by Equations (13,14). That is,

$$F_1 = tanh\left\{\left[min\left[max\left(\frac{\sqrt{k}}{0.09\omega y}, \frac{500v}{y^2\omega}\right), \frac{4\rho\sigma_{\omega 2}k}{CD_{k\omega}y^2}\right]\right]^4\right\} \tag{13}$$

In which, $CD_{k\omega}$ is defined by,

$$CD_{k\omega} = max\left(2\rho\sigma_{\omega 2}\frac{1}{\omega}\frac{\partial k}{\partial x_j}\frac{\partial \omega}{\partial x_j}, 10^{-20}\right) \tag{14}$$

The k-ω SST turbulence model constants are mentioned in Table 1 [6],

Table 1 K-ω SST turbulence model constants [6]

K-ω SST turbulence model constants	Value
β^*	0.09
β_1	0.075
β_2	0.0828
γ_1	0.5532
γ_2	0.4404
σ_{k1}	0.85
σ_{k2}	1.0
$\sigma_{\omega 1}$	0.5
$\sigma_{\omega 2}$	0.856

2.3. Flow Separation Control using the Plasma (DBD)

The continuity equation for each component i in plasma is obtained from the Boltzmann equation, which is as Equation (15), [14-17].

$$\frac{\partial n_i}{\partial t} + \nabla.\Gamma_i = S_i \tag{15}$$

In this equation n_i is the density of component i, Γ_i is the flux i, and S_i is a source term that shows the rate of change of density i caused by chemical reactions and is calculated as Equation (16), [14-17].

$$s_i = \sum_r C_{i,r} R_{i,r} = \sum_r \left[C_{i,r} K_r \prod_j n_j \right] \tag{16}$$

In Equation (16) r is the underscore for production or dissipation reaction for i, $c_{i,r}$ is the stoichiometric coefficient i in reaction r, $R_{i,r}$ is the reaction rate, K_r is reaction rate coefficient, and the underscore j is related to the reacting components. In Equation (15) the drift-diffusion approximation is used to calculate the flux. Considering the effects of ambient fluid velocity, the flux relationship for electrons, ion components, and neutral components are obtained as Equations (17)-(19) respectively [14-17].

$$\vec{\Gamma}_e = -\mu_e n_e \vec{E} - D_e \vec{\nabla} n_e + n_e \vec{V} \tag{17}$$

$$\vec{\Gamma}_i = -\mu_i n_i \vec{E} - D_i \vec{\nabla} n_i + n_i \vec{V} \tag{18}$$

$$\vec{\Gamma}_{uc} = -D_{uc} \vec{\nabla} n_{uc} + n_{uc} \vec{V} \tag{19}$$

In the above relationships $\vec{E}$ is the electric field, μ_i is the electrical excitability and D_i is the diffusion coefficient for component i. Mobility and diffusion coefficients are determined by the interactions between the components and the background gas, with the following equations respectively [14-17].

$$\mu_i = \frac{q_i}{m_i v_i} \tag{20}$$

$$D_i = \frac{k_B T_i}{m_i v_i} \tag{21}$$

In the above equations q_i is the electric charge of component i, m_i is the mass of component i, v_i is the contact frequency for the momentum of component i with the foreground gas, k_B is the Boltzmann constant, and T_i is the temperature of component i. Heavy particles are assumed to be in equilibrium with the foreground gas, so there is no need to solve the energy equation for these particles and the energy relation is solved for electrons only. This relation for electrons is in the form of Equation (22), [14-17].

$$\frac{\partial n_\varepsilon}{\partial t} + \nabla.\Gamma_\varepsilon = S_\varepsilon \tag{22}$$

In this respect n_ε is the density of electron energy, which is defined as $n_\varepsilon = n_e \bar{\varepsilon}$, and $\bar{\varepsilon}$ is the average energy of electrons associated with the temperature of electrons through Equation (23), [15-18].

$$k_b T_e = \frac{2\bar{\varepsilon}}{3} \tag{23}$$

And also, the electron energy flux can be calculated from Equation (24) [14-17],

$$\vec{\Gamma}_\varepsilon = -\frac{5}{3}\mu_e n_\varepsilon \vec{E} - \frac{5}{3} D_e \vec{\nabla} n_\varepsilon + n_\varepsilon \vec{v} \tag{24}$$

The source term is derived from the energy equation according to Equation (25). The additional part of this term is due to the ohmic electron heating by electric field [14-17].

$$S_\varepsilon = -e\Gamma_e . E - n_e \sum_r \bar{\varepsilon}_r K_r n_r \tag{25}$$

The two right terms represent the heat generated by the electric field and the electron energy loss due to the collision, respectively. Parameter of r denotes the reactions associated with the electron collision. n_r is the density of the target component and $\bar{\varepsilon}_r$ is the reaction threshold energy. Using the Gauss law, the electric field is related to the charge density through Equation (24) [14-17],

$$\nabla . (\epsilon E) = -\nabla . (\epsilon \nabla \phi) = \rho_c \tag{26}$$

The charge density can also be calculated as follows,

$$\rho_c = \sum_i q_i n_i \tag{27}$$

Finally, the electro-hydrodynamic force applied to the fluid due to the electric field and the charged particles in the fluid can be calculated by means of Equation (28), [14-17].

$$\vec{F}_{EHD} = \rho_c \vec{E} = -\nabla \Phi \sum_i q_i n_i \tag{28}$$

2.4. Navier Stokes-plasma equation

For fluid flow, the continuity Equation (27) and momentum Equation (28) are solved in both *x* and *y* directions, and since in non-heat plasma the gas temperature remains at ambient temperature, thus there is no need to solve the energy equation for fluid. In this respect, ρ and v are density and velocity vectors, respectively.

$$\frac{\partial \rho}{\partial t} + \nabla . (\rho V) = 0 \tag{29}$$

The momentum equation for the incompressible state, known as the Navier-Stokes equation, is expressed as Equation (30).

$$\rho \left(\frac{\partial v}{\partial t} + v . \nabla v \right) = -\nabla p + \mu \nabla^2 v + F_{EHD} \tag{30}$$

In this relation, P is pressure, μ is fluid dynamic viscosity, and F_{EHD} is the volumetric force caused by the plasma phenomenon (per unit volume) [9].

2.5. Computing Space and Meshing

The purpose is to check the flow near an airfoil. For this purpose, the computational space must first be plotted and then meshed and boundary conditions specified, and after numerically solving the equations, the results are extracted. Fig. 2 illustrates the computational space with meshing, which includes boundary conditions as flow inlet, flow outlet, and airfoil wall. In order to obtain better information about the areas around the airfoil, the meshing around the airfoil is presented in the following Fig. 2. As shown, a finer mesh is used near the airfoil, as the computation accuracy in these areas should be greater.
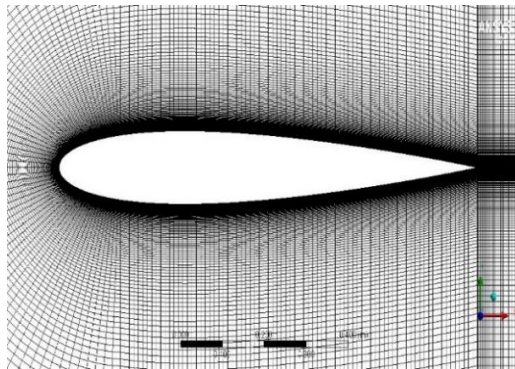
Fig. 2 Meshing around NACA 0012 Airfoil.

Also, Table 2 provides details of the meshing parameters,

Table 2 The meshing parameters

Number of meshing elements	48800
Number of nodes	48412
Minimum orthogonal quality	5.67×10^{-3}
Maximum aspect ratio	1.72×10^3

2.6. Boundary Conditions

In this study, the Reynolds number of 3×10^6 is assumed for the flow around the airfoil, as shown in Equation (31) and Table 3 [10].

$$Re = \frac{\rho \, v \, C}{\mu} \tag{31}$$

Where ρ is the air density, v is the velocity of the flow, c is the chord length of the airfoil and μ is the dynamic viscosity of the air. Also, the problem definition and flow simulation method using Ansys Fluent software is as follows. Reference parameters for the present research are as Table 3.

Table 3 Reference Parameters

Parameter	Value	Symbol	Unit
Reynolds number	-	Re	-
Air density	1.225	ρ	kg/m^3
dynamic viscosity	1.78×10^{-5}	μ	kg / m-s

Airfoil chord length	1	C	m
Flow velocity	44	v	m/s

Also presented in Table 4, are input data for simulation in ANSYS Fluent software,

Table 4 Input data for simulation in ANSYS Fluent software

Computation space	2D
Time dependence	Steady
Turbulence model	$k - \omega\ SST$
Turbulence viscosity ratio	10
Temperature	300 K
Pressure	101325 Pa

Tables 3 and 4 are related to the solution of flow field. That is, the plasma is inactive. With the addition of plasma, which is written in the C programming language, it is defined as a body force compiled in ANSYS Fluent software.

3. Results and Discussions

A few topics was reviewed including the study of flow around NACA 0012 airfoil, calculation and comparison of lift coefficients in plasma off and plasma on modes, specification of the angle of stall and also minimizing return flows and eddies using plasma actuators, and the results of each of the obtained variables were evaluated.

3. 1. Investigating the Speed Contour in Active Plasma and Inactive Plasma Modes

According to Fig. 3, the fixed airfoil and the angle of attack of 10º and 16º on the flow line are given in plasma off and on modes. As shown in Figs. 3(a), (b) as the flow angle increases in plasma off mode, the flow separation area increases and eddies and return flows increase. Figs. 3(c), (d) show that with the help of plasma actuator, the current separation region is delayed at these angles and also the eddies and return flows are minimized.
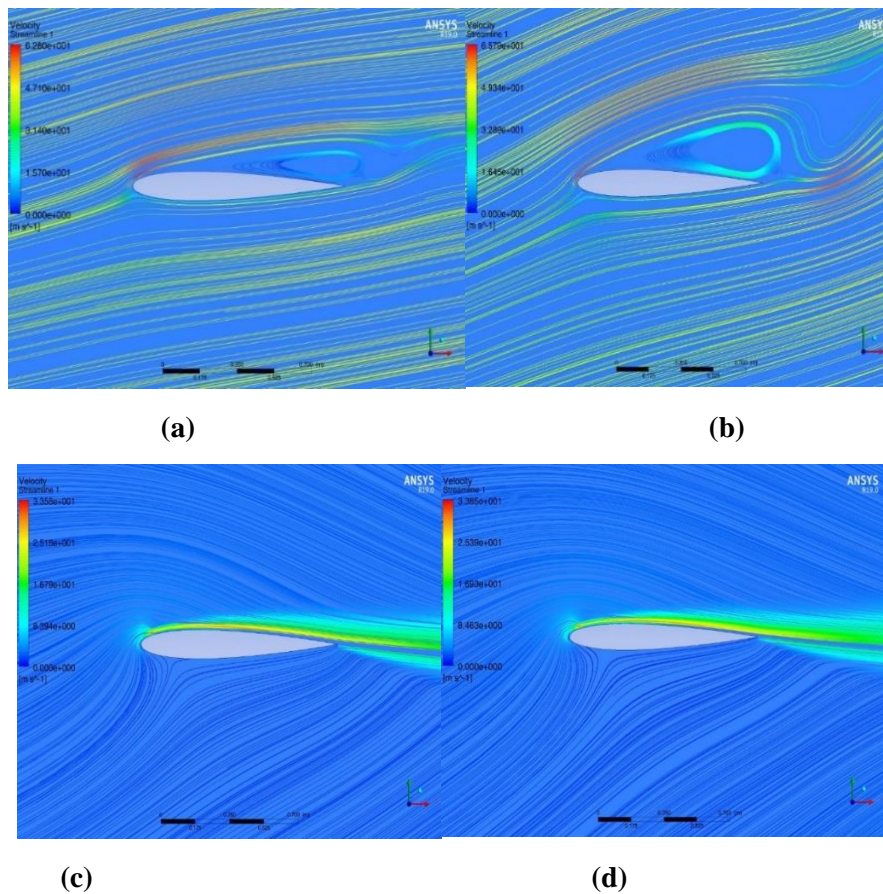
Fig. 3 (a) Flow velocity contour at angle of attack of 10° (plasma off) (b) Flow velocity contour at angle of attack of 16° (plasma off) (c) Flow velocity contour at angle of attack of 10° (plasma on) (d) Flow velocity contour at angle of attack of 16° (plasma on)

3. 2. Investigating the Lift Coefficients and Stall Angle in Plasma-on and Plasma-off Modes

The obtained results of the lift coefficients in plasma off and plasma on modes are compared with the numerical results of K-ω SST and Spalart-Allmaras results [11] (see Figs. 4, 5). Based on Fig. 4, the maximum lift coefficient (Max-C_l: stall angle) at Reynolds 3×10^6 in plasma off mode is similar to that of the stall angle of K-ω SST and Spalart-Allmaras models [11]. And also Fig. 4 illustrates that the stall angle of the turbulence model used in present study in Plasma off mode and the stall angles K-ω SST and Spalart-Allmaras models [11] happens at an angle 16°. According to the results of lift coefficients in the stall angle regions, K-ω SST-Plasma off model shows the similar results compared to stall angle regions lift coefficients of the K-ω SST model [11]. It has also been shown that in Plasma On mode, the stall angle has a delay from 16º to 19º angle of attack.
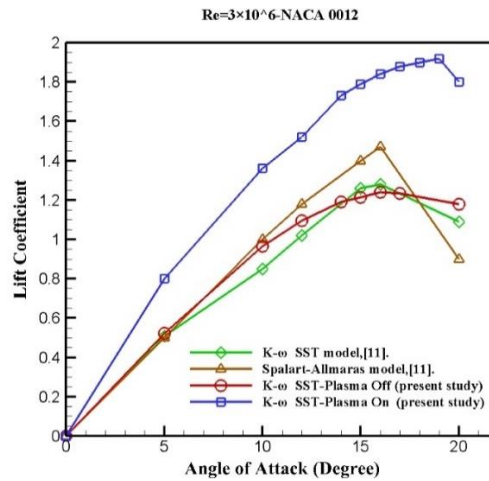
Fig. 4 Comparison of the obtained results with available data [11] for analyzing (predicting) lift coefficients C_l

As shown in Fig. 5, the lift coefficients and critical angles (stall) using K-ω SST-Plasma off model have been compared with the experimental results [11,19]. Based on Fig. 5, the stall angle (Max-C_l) in the numerical results of the present study and the stall angles presented in the experimental results [11,19] occur in the attack angle of 16°. In addition, the experimental results [19] show the highest value of the lift coefficients. As well, the experimental results [11] show the lowest value of the lift coefficients compared with the K-ω SST-Plasma off model.
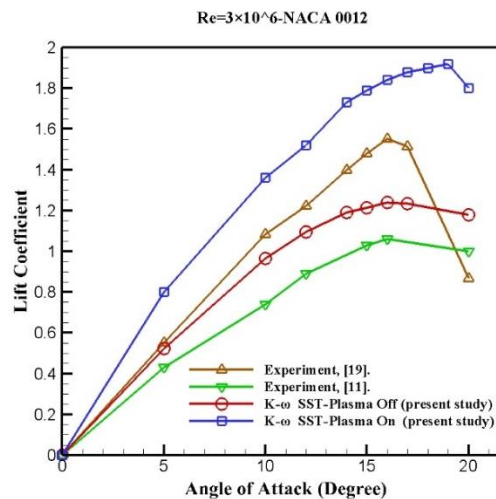

Fig. 5 Prediction and comparison of lift coefficients C_l in various states

Figs. 4 and 5 present an important and interesting data and information regarding the lift coefficients C_l in various states. Also, meaningful agreements are found through comparing the obtained (predicted) and available results [11,19].

4. Conclusions

The following results and conclusions are found by the present research work,

- In the plasma off state, with increasing the angle of attack, the flow separation region, eddies, and return flows increased. By defining plasma (DBD) as a body force, the flow separation region is decreased at high angle of attacks and critical angles. In which, the return flows (eddies) are minimized behind the airfoil.

- The stall angles of Plasma Off mode are the same as the stall angles of K-ω SST and Spalart-Allmaras models [11], and stall angles of all three models (Max-C_l) occur at an angle of attack of 16$^\text{o.}$

- The K-ω SST- Plasma off model lift coefficients are the closest to the K-ω SST model [11] lift coefficients compared with the Spalart-Allmaras model lift coefficients [11].

- The obtained results of K-ω SST model (Plasma Off) are closer to the experimental results [19] compared with the experimental data [11]. For validation, the obtained results of the present study are between the available experimental data [11,19].

- Using this actuator in the optimum position on the NACA 0012 airfoil (at place of flow separate with Reynolds number of 3×10^6) the stall angle delayed from a 16$^\text{o}$ angle of attack at normal state to a 19$^\text{o}$ angle of attack.

- In plasma (DBD) On mode, airflow control over the airfoil is significantly improved, therefore the aircraft control is improved at critical angles.

- Finally, use of two or three plasmas in different parts of the airfoil can be beneficial for better controlling the flow and pressure on the airfoil.

References

[1] E. Esmaeilzadeh, M. Aghazeinali., "Numerical investigation of fluid flow around circular cylinder affected by an electro hydrodynamic (EHD) flush mounted wire plate actuator", Journal of Faculty of Eng, Vol. 32, No. 2, 1-19, 2006.

[2] L. Leger, E. Moreau, G. Artana, G. Touchard., "Influence of a DC corona discharge on the airflow along an inclined fat plate", Journal of Electrostatics, Vol. 51-52, pp. 300-306, 2001.

[3] G. Artana, R. Sosa, E. Moreau, G. Touchard., "Control of the near-wake flow around a circular cylinder with electrohydrodynamic actuators", Experiments in Fluids 35 (2003) 580–588

[4] A. Salmasi, A. Shadaram, M. Mirzaei, A. Sh. Taleghani., "Numerical and experimental investigation on the effect of a plasma actuator on NLF0414 airfoil's efficiency after the stall", Modares Mechanical Engineering, Vol. 12, No. 6, pp. 104-116, 2013. URL: http://mme.modares.ac.ir/article-15-5553-en.html

[5] Anderson J.D. Jr. (2010) FUNDAMENTALS OF AERODYNAMICS, FIFTH EDITION, McGraw-Hill series in aeronautical and aerospace engineering, Chapter4: Incompressible Flow over Airfoils.

[6] Florian R. Menter., "Improved Two-Equation k-ω Turbulence Models for Aerodynamic Flows", NASA National Aeronautics and Space Administration, October 1992, PP. 3-11

[7] Stephen B. Pope, "Turbulent flows", Cambridge University Press, year: 2000, pp. 383-387

[8] Modeling Turbulent Flows., "Introductory FLUENT Notes FLUENT v6.3 December 2006", Fluent User Services Center, www.fluentusers.com

[9] Babou, Y., E. Martin and P. Peña., "Simple body force model for Dielectric Barrier Discharge plasma actuator", 7TH EUROPEAN CONFERENCE FOR AERONAUTICS AND AEROSPACE SCIENCES (EUCASS), DOI: 10.13009/EUCASS2017-122

[10] R. H. BARNARD, D. R. PHILPOTT., "Aircraft Flight", A description of the physical principles of aircraft flight, Fourth Edition, pp. 361-362

[11] B. Raghava Rao, Rangineni Sahitya., "Numerical and Experimental Investigation of the Flow Field Around NACA 0012 Aerofoil", International Journal on Theoretical and Applied Research in Mechanical Engineering (IJTARME), Issue 4, 2015, pp. 18-26.

[12] B Jayaraman, YC Cho, W Shyy., "Modeling of Dielectric Barrier Discharge Plasma Actuator", Journal of Applied Physics 103, 1-15, 053304 (2008). DOI: 10.1063/1.2841450

[13] K Asada, Y Ninomiya, A Oyama, K Fujii., "Airfoil Flow Experiment on the Duty Cycle of DBD Plasma Actuator", American Institute of Aeronautics and Astronautics, 2009, pp. 1-14.

[14] Nagaraja, S., V. Yang, and I. Adamovich., "Multi-scale modelling of pulsed nanosecond dielectric barrier plasma discharges in plane-to-plane geometry", Journal of Physics D: Applied Physics, vol 46, 2013, pp. 155-205.

[15] Antonio Castellanos (2014)., Electrohydrodynamics, Springer, pp. 56-72.

[16] Jayaraman, B., S. Thakur and W. Shyy., "Modeling of Fluid Dynamics and Heat Transfer Induced by Dielectric Barrier Plasma Actuator", J. Heat Transfer, Apr 2007, 129(4): 517-525.

[17] Thamir H. Khalaf and Zainab D. Abd Ali., "Computational Diagnostics for Dielectric Barrier Discharge plasma", Journal of Al-Nahrain University, Vol 18 (4), December, 2015, pp. 67-74.

[18] John S. Duncan (2016), "Pilot's Handbook of Aeronautical Knowledge", U.S. Department of Transportation FEDERAL AVIATION ADMINISTRATION Flight Standards Service, Chapter 5: Aerodynamics of Flight, pp. 25-32.

[19] Abbott IH, Von Doenhoff AE (1959), "Theory of Wing Sections "Dover Publishing, New York

[20] M Bigdeli, V Monfared, Investigation and Comparison of Stall Angle of Airfoil NACA 0012 in Reynolds Number of 3×10^6 with K ω SST, Realizable k ε, Spalart-Allmaras Turbulence Models, Comptes Rendus de l 'Academie Bulgare des Sciences, Proceedings of the Bulgarian Academy of Sciences, 2020, 73(3), 394-402.